Ab initio charge-carrier mobility model for amorphous molecular semiconductors

Andrea Massé,[1,*] Pascal Friederich,[2] Franz Symalla,[2] Feilong Liu,[1] Robert Nitsche,[3] Reinder Coehoorn,[1,4] Wolfgang Wenzel,[2] and Peter A. Bobbert[1]

[1]*Department of Applied Physics, Technische Universiteit Eindhoven, P.O. Box 513, NL-5600 MB Eindhoven, The Netherlands*

[2]*Institute of Nanotechnology, Karlsruhe Institute of Technology (KIT), D-76344 Eggenstein-Leopoldshafen, Germany*

[3]*sim4tec GmbH, Arnoldstrasse 18b, D-01307 Dresden, Germany*

[4]*Institute for Complex Molecular Systems, Technische Universiteit Eindhoven, P.O. Box 513, NL-5600 MB Eindhoven, The Netherlands*

(Received 14 January 2016; revised manuscript received 2 May 2016; published 19 May 2016)

Accurate charge-carrier mobility models of amorphous organic molecular semiconductors are essential to describe the electrical properties of devices based on these materials. The disordered nature of these semiconductors leads to percolative charge transport with a large characteristic length scale, posing a challenge to the development of such models from *ab initio* simulations. Here, we develop an *ab initio* mobility model using a four-step procedure. First, the amorphous morphology together with its energy disorder and intermolecular charge-transfer integrals are obtained from *ab initio* simulations in a small box. Next, the *ab initio* information is used to set up a stochastic model for the morphology and transfer integrals. This stochastic model is then employed to generate a large simulation box with modeled morphology and transfer integrals, which can fully capture the percolative charge transport. Finally, the charge-carrier mobility in this simulation box is calculated by solving a master equation, yielding a mobility function depending on temperature, carrier concentration, and electric field. We demonstrate the procedure for hole transport in two important molecular semiconductors, α-NPD and TCTA. In contrast to a previous study, we conclude that spatial correlations in the energy disorder are unimportant for α-NPD. We apply our mobility model to two types of hole-only α-NPD devices and find that the experimental temperature-dependent current density–voltage characteristics of all devices can be well described by only slightly decreasing the simulated energy disorder strength.

DOI: 10.1103/PhysRevB.93.195209

I. INTRODUCTION

Amorphous organic molecular semiconductors play a central role in the active layer of various types of organic optoelectronic devices, such as organic light-emitting diodes (OLEDs), organic photovoltaic (OPV) devices, and light-emitting organic field-effect transistors (LEOFETs). Their importance has led to extensive efforts to study charge transport in these materials, which occurs by incoherent hopping of charge carriers between molecular sites with random energies. The most important parameter characterizing the transport is the charge-carrier mobility μ. In the early modeling, the random energies were described by a Gaussian density of states (DOS) [1], leading to the Gaussian disorder model (GDM). In the GDM, it is assumed that there is no spatial correlation between the site energies. It was suggested, however, that the presence of dipole moments in organic semiconductors can give rise to spatial correlation between the site energies [2,3], leading to the correlated disorder model (CDM). Later, it was realized that, apart from the dependence of μ on temperature T and electric field F, there is a strong dependence on the carrier concentration c [4–11], giving rise to extended versions of the GDM and CDM, the EGDM and ECDM, respectively. Percolation effects in the charge transport inherent to disordered systems, which become dominant at low T, are fully accounted for in the EGDM and ECDM. The EGDM and ECDM provide parametrizations of the mobility function $\mu(T,c,F)$ that can be readily used in drift-diffusion modeling of charge transport in organic devices.

The key parameters in both the EGDM and ECDM are the strength of the energetic disorder, quantified by the standard deviation σ of the DOS, and the site density N_t. In the limit of vanishing c and F, both the EGDM and ECDM yield a temperature dependence that can be described by $\mu \propto \exp(-C\hat{\sigma}^2)$ in the range of values $2 \leqslant \hat{\sigma} \leqslant 6$ important for applications, where $\hat{\sigma} \equiv \sigma/k_B T$. For the EGDM a value $C = 0.42$ is obtained [7], whereas the ECDM yields $C = 0.29$ [9]. Another important difference is that the ECDM predicts a much stronger F dependence than the EGDM. The c dependence of both models was shown to be essentially the same [11]. Good agreement between measured T-dependent current density–voltage (J-V) characteristics of hole-only devices of α-NPD [N,N′-Di(1-naphthyl)-N,N′-diphenyl-(1,1′-biphenyl)-4,4′-diamine] and those calculated with both the EGDM and ECDM could be obtained, but with different values of σ and N_t: $\sigma = 0.14$ eV, $N_t = 0.20 \times 10^{27}$ m^{-3} for the EGDM and $\sigma = 0.10$ eV, $N_t = 3.7 \times 10^{27}$ m^{-3} for the ECDM [12]. Because for the ECDM N_t was closer to the actual density of molecules than for the EGDM, it was suggested that site energies in α-NPD are spatially correlated.

The mobility functions $\mu(T,c,F)$ previously obtained for the EGDM and ECDM were based on simulations of charge transport on cubic lattices with Miller-Abrahams hopping rates [13], depending only on the energy differences between the sites and a spatially exponentially decreasing coupling prefactor reflecting the decay of the localized wave functions. The wave function decay length was assumed to be so short that essentially only nearest-neighbor hopping was accounted for [7,9]. So far, the influence of the system-dependent morphology on the spatial decay and variations of the intersite coupling (off-diagonal disorder [10,14]) and hence

*a.masse@tue.nl

on the mobility function has only been scarcely addressed in literature. In a fully predictive approach the mobility function for a particular molecular semiconductor should follow from *ab initio* microscopic simulations of the morphology and hopping rates. In the last few years, some research groups have started to follow this road [15–20]. The improvements expected from such an approach include quantified insight in the role of the spatial decay and off-diagonal disorder of the intersite coupling.

Recently, a generalized effective-medium model (GEMM) based on such *ab initio* simulations was developed to determine the T and F dependencies of the hole mobilities of α-NPD and Alq_3 [tris(8-hydroxyquinolinato)aluminium] in the limit of low c [21]. In this model, the value $C = 0.25$ is obtained. The simulated values of σ were 0.130 eV (α-NPD) and 0.227 eV (Alq_3), with the former value close to the EGDM value found in the modeling of α-NPD devices [12], but incompatible with the ECDM value. The GEMM prediction of the T dependence of the mobilities was found to agree rather well with experiment, even at low T. This is surprising, because the GEMM does not take into account percolation effects.

In an attempt to resolve this puzzling situation, we develop in the present paper a charge-carrier mobility model based on *ab initio* microscopic simulations of the morphology and hopping rates that at the same time fully captures percolation effects. Large system sizes are required to capture such effects [22]. In *ab initio* simulations this poses a major problem, because of the exceedingly high computational costs involved. Recently, stochastic models have been developed that can be used to extrapolate *ab initio* microscopic information about the morphology and charge-transfer integrals obtained from simulation boxes of relatively small sizes, containing on the order of a thousand molecules, to generate realistic morphologies and hopping rates for arbitrarily large systems [23,24]. We will employ such models in this work. An equally puzzling situation we wish to resolve is the suggestion that correlated disorder would be relevant for charge transport in α-NPD [12], while the α-NPD molecule has no static dipole moment.

The paper is organized as follows. In Sec. II we develop our mobility model and demonstrate it for hole transport in α-NPD and TCTA [tris(4-carbazoyl-9-ylphenyl)amine]. Both are important materials used in OLEDs as hole transporting and/or guest material in dye-doped light-emitting layers [25]. The model is based on *ab initio* microscopic simulations of the morphology and hopping rates as described in Refs. [18,19,21]. We discuss and apply the stochastic model employed to extrapolate the *ab initio* microscopic information to large systems. Results are given for the T, c, and F dependencies of the hole mobility μ of α-NPD and TCTA, obtained by solving a master equation for the site occupation probabilities of large systems. Parametrizations are given for these dependencies that can be conveniently used in device simulations. In Sec. III we apply the mobility function $\mu(T,c,F)$ for α-NPD to describe the J-V characteristics of two types of α-NPD hole-only devices. The first type has doped injection layers with a negligible injection barrier. The second type has ITO (indium tine oxide) as anode material, leading to a considerable injection barrier. In Sec. IV we discuss our results and present our conclusions.

II. *AB INITIO* MOBILITY MODEL

In this section we develop an *ab initio* model for the charge-carrier mobility in amorphous molecular semiconductors, which we will apply to hole transport in α-NPD and TCTA. Charge transport in such semiconductors occurs by incoherent hopping with a rate ω_{ij} between two electronically weakly coupled molecular sites i and j, for which we will take the Marcus formula [26]

$$\omega_{ij} = \frac{2\pi}{\hbar}\frac{J_{ij}^2}{\sqrt{4\pi E_\mathrm{r} k_\mathrm{B} T}}\exp\left[-\frac{(\Delta E_{ij} - E_\mathrm{r})^2}{4E_\mathrm{r}k_\mathrm{B}T}\right]. \quad (1)$$

Here, E_r is the molecular reorganization energy. $\Delta E_{ij} \equiv E_j - E_i$ and J_{ij} denote the energy difference and the charge-transfer integral between sites i and j, respectively. The energy difference ΔE_{ij} contains a contribution $-eFR_{ij,x}$ due to an electric field F applied in the x direction, where $R_{ij,x}$ is the pair distance along this direction and e the unit charge.

We use a multiscale modeling approach to obtain the hopping rates for a mesoscopic system from *ab initio* simulations of a microscopic system. The *ab initio* microscopic site positions, site energies, transfer integrals, and reorganization energies for holes were obtained as follows. Morphologies were obtained using the DEPOSIT code, which was applied to simulate deposition of about 900 molecules in the vertical direction in simulation boxes of a lateral size of 10×10 nm^2 with periodic boundary conditions in the lateral directions [18]. Site positions, defined as the molecular centers of mass, were obtained from a slab of this box with a height of 6.5 nm, avoiding surface effects. The resulting site densities are $N_\mathrm{t} = 0.96 \times 10^{27}$ and 0.87×10^{27} m^{-3} for α-NPD and TCTA, respectively. Site energies were obtained using the quantum patch embedding method described in Ref. [19]. Transfer integrals were calculated based on self-consistently evaluated molecular frontier orbitals using the Löwdin orthogonalization [27,28]. The Fock and overlap matrices were extracted from dimer calculations including environment embedding. Both site energies and transfer integrals were calculated with the Turbomole package [29] using a B3LYP functional [30] and a def2-SV(P) basis set [31]. The reorganization energies were calculated using Nelsen's four-point procedure [32] with a B3LYP functional and a def2-TZVP basis set in Turbomole [33]. In the calculations of the site energies, transfer integrals, and reorganization energies, the morphology simulation boxes were periodically repeated in the lateral directions. A spherical subsystem of about 3500 molecules was then considered, which was used as an electrostatic background for about 1000 molecules in the center of this subsystem, for which the calculations were performed self-consistently. The resulting site energies for holes are in very good approximation distributed according to a Gaussian DOS with $\sigma = 0.130$ and 0.136 eV for α-NPD and TCTA, respectively. The reorganization energies of the molecules for holes vary only by about 0.05 eV around the values $E_\mathrm{r} = 0.203$ and 0.257 eV, respectively, and we fix them at the latter values in the following.

In Fig. 1 we investigate the spatial correlation in the site energies of the *ab initio* simulations. We take a central site with a certain energy E_i and consider the energies E_j of all sites within a sphere with radius R around that site. Without spatial correlation between the energies the average

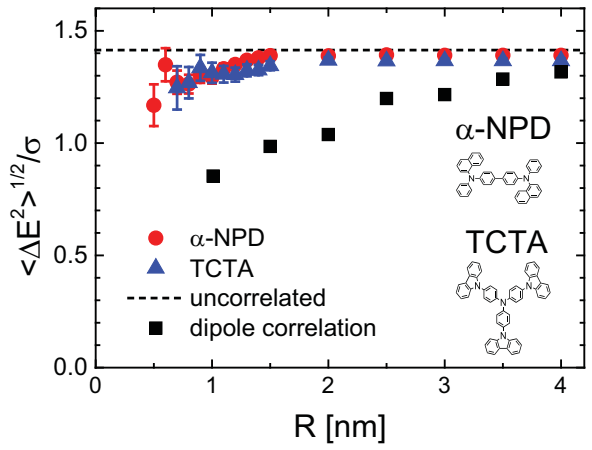

FIG. 1. Degree of correlation between the hole energy at a molecular site and the hole site energies within a sphere of radius R around that site, for *ab initio* microscopic simulations of α-NPD and TCTA (molecular structures in the inset). The results are averages over 7 and 3 samples, respectively, of about 1000 molecules. Results are also shown for spatially uncorrelated energy disorder and energy disorder due to randomly oriented dipoles on a cubic lattice.

$\langle \Delta E^2 \rangle^{1/2} \equiv \langle (E_i - E_j)^2 \rangle^{1/2}$ is equal to $\sqrt{2}\sigma$ (dashed line). The deviation from this value is a measure for the degree of correlation. We also plot $\langle \Delta E^2 \rangle^{1/2}$ for the case of energy disorder due to the electrostatic potential of randomly oriented dipoles on the sites of a cubic lattice with a lattice constant of 1 nm (squares). It is clear from Fig. 1 that the energy disorder in both α-NPD and TCTA is almost completely uncorrelated. We note that in Alq_3 a strong spatial correlation was found [23]. The difference can be attributed to the large molecular dipole moment of the Alq_3 molecule, in contrast to the vanishing dipole moments of α-NPD and TCTA molecules. Figure 1 shows that hole transport in α-NPD and TCTA should be described with uncorrelated energy disorder, at variance with the suggestion of Ref. [12] that site energies in α-NPD are spatially correlated.

A. Stochastic model for the morphology

In order to capture percolative effects at low temperature, the description of hole transport in α-NPD and TCTA requires very large simulation boxes, for which *ab initio* simulations are computationally unfeasible. Instead, we use a stochastic model similar to that in Ref. [23] to extrapolate morphology information obtained from *ab initio* microscopic simulations in small boxes to arbitrarily large boxes.

We define a morphology to be a set of points in a box representing molecular centers of mass. We will require that the stochastic model reproduces the nearest-neighbor (NN) distance probability distribution function (PDF) of the *ab initio* morphology simulations in the small box. In particular, since the molecules have a finite extension, the molecular centers of mass have a minimum NN distance that should be reproduced by the stochastic model. Also, the site density N_t of molecules should be reproduced. In order to meet these requirements, we use a dominance-competition point-process model similar to that developed by Baumeier *et al.* [23], which is based on the thinning of a Poisson process. We first choose a random number N from the Poisson distribution with average $N_t V$, where V is the volume of a large simulation box. We randomly and uniformly distribute N points over that box. In order to account for the finite extension of the molecules, a spherical volume with a random radius r_i is assigned to each site i, where $r_i \sim \Gamma(k,\theta) + r_h$ is a random distance drawn from a gamma distribution with shape k and scale θ, shifted over a distance r_h. The shift over r_h takes account of the minimum NN distance. Whenever the site i is located within the sphere around site j or/and vice versa (the sites are "in competition"), the site with the smallest sphere is removed. This leads to a density $N_t' < N_t$, but then a number N' of new sites is chosen from the Poisson distribution with average $(N_t - N_t')V$ that are randomly distributed over the left empty space between the spheres. To these new sites the same thinning procedure is applied, with a difference that when a new site is in competition with an existing site, the new site is removed. This process is repeated until the relative change in the density of sites is less than 10^{-6}, which in our case leads to about ten iterations.

Baumeier *et al.* applied their procedure to Alq_3 and could reproduce the (cumulative) NN distance PDF, the pair correlation function (PCF), and the spherical contact distribution function all rather well using the same parameter set [23]. In our case, we focus solely on reproducing the NN distance PDF, since this function should be the most relevant for the charge transport. In Figs. 2(a) and 2(b) we compare histograms of the stochastically

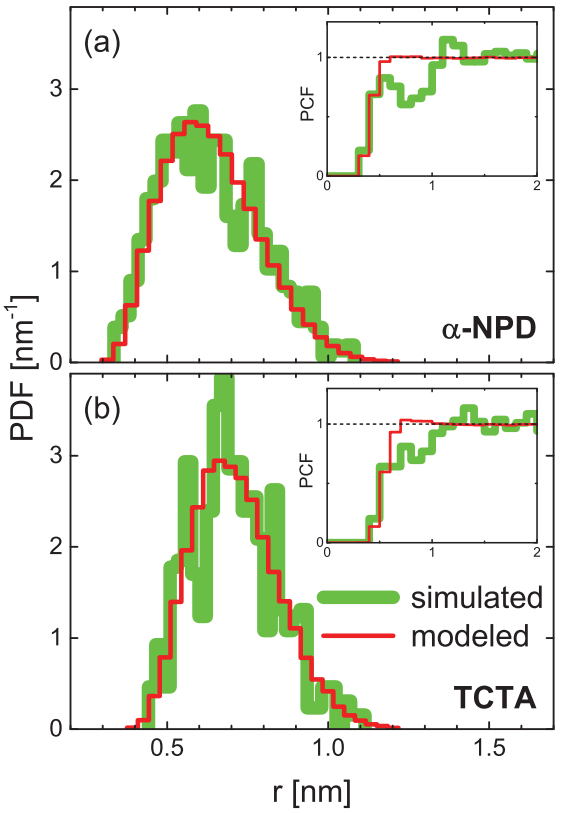

FIG. 2. Main panels: Histograms of the nearest-neighbor (NN) distance probability distribution functions (PDFs) of a simulated (modeled) morphology in a box of $10 \times 10 \times 6.5$ ($50 \times 50 \times 50$) nm^3, containing about 600 (100 000) NN pairs for (a) α-NPD and (b) TCTA. Insets: Corresponding pair correlation functions (PCFs).

modeled to the *ab initio* simulated NN distance PDF for α-NPD and TCTA, respectively. The used parameters are $r_h = 0.25$ nm, $k = 3.40$, $\theta = 0.040$ nm (α-NPD) and $r_h = 0.32$ nm, $k = 3.85$, $\theta = 0.047$ nm (TCTA). As can be observed, the stochastic model provides a very good description of the NN distance PDFs. The insets in Figs. 2(a) and 2(b) give a similar comparison of the PCFs. We observe that features in the PCFs of the simulated morphologies beyond the typical NN distance of ~0.6 nm are not properly described by the stochastic model. We attribute these features to anisotropic local packings of the α-NPD and TCTA molecules, which, unlike the Alq_3 molecule, have a strongly nonspherical shape. Taking into account anisotropic packings would require an elaborate extension of the present isotropic stochastic model of which we do not expect an important effect on the final mobility function.

B. Stochastic model for the transfer integrals

Our procedure for the stochastic modeling of the transfer integrals is different from that of Baumeier *et al.* [23], who found for Alq_3 to a very good approximation at each distance a log-normal distribution of the squared transfer integrals. The strongly nonspherical shape of the α-NPD and TCTA molecules leads to more complicated distributions that cannot be described with a simple parametrization scheme. Instead, we proceed as follows. First, we divide the distance interval within which all considered *ab initio* transfer integrals J_{ij} between sites i and j are found into K equal bins labeled by k. For each distance bin k we divide the interval in which all values of $\ln(J_{ij}^2/\mathrm{eV}^2)$ are found (with R_{ij} in distance bin k) in M equal transfer-integral bins labeled by m. Next, we associate to all transfer-integral bins the appropriate transfer integrals $J_{m,k}$ and statistical (nonnormalized) weights $w_{m,k}$ determined by

$$w_{m,k} = \sum_{\langle ij\rangle \in k} \exp\left[-\frac{\left\{ \ln\left(J_{ij}^2/\mathrm{eV}^2\right) - \ln\left(J_{m,k}^2/\mathrm{eV}^2\right)\right\}^2}{2\sigma_k^2} \right], \quad (2)$$

where $\langle ij\rangle \in k$ are a pair of sites with R_{ij} in distance bin k and σ_k is a smoothing parameter chosen such that the $J_{m,k}$'s provide an accurate yet smooth sampling of the rather small set of *ab initio* simulated J_{ij}'s in each distance bin k. Finally, for each pair of sites in the stochastically modeled morphology the appropriate distance bin k is determined and a transfer integral $J_{m,k}$ is randomly chosen according to the weights $w_{m,k}$. Pairs with a separation larger than the longest distance considered in the *ab initio* simulations are given a zero transfer integral.

Figures 3(a) and 3(b) are scatter plots of the *ab initio* simulated hole transfer integrals in samples of α-NPD and TCTA, respectively. We observe that the spread in the transfer integrals for TCTA is much larger than for α-NPD, which is caused by the very different molecular structure. We note that Fig. 3 only shows the transfer integrals of pairs of molecules for which the closest atom-atom distance is smaller than 1 nm. For a larger closest distance the HOMO (highest occupied molecular orbital) overlap of the two molecules is negligible and hence the transfer integral does not need to be calculated.

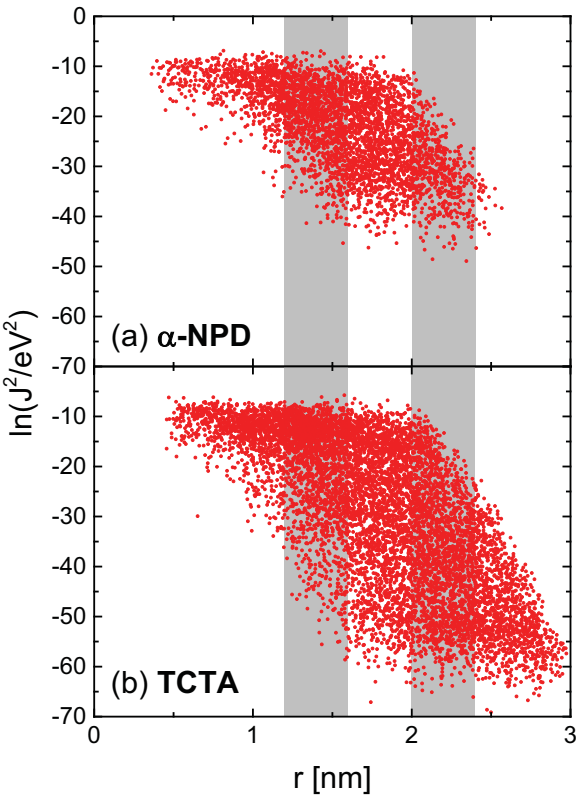

FIG. 3. *Ab initio* simulated values $\ln(J^2/\mathrm{eV}^2)$ of the transfer integrals J between molecules at a distance r between their centers of mass, for samples of (a) α-NPD (about 4000 transfer integrals) and (b) TCTA (about 8000 transfer integrals).

In the stochastic modeling of the transfer integrals we considered distance intervals of 0.36–2.57 nm (α-NPD) and 0.46–2.97 nm (TCTA), and $K = 100$ distance as well as $M = 100$ transfer-integral bins. We chose the smoothing parameter σ_k equal to five times the transfer-integral bin size for each distance bin k. In Fig. 4 we compare histograms of the stochastically modeled to the *ab initio* simulated PDFs of the transfer integrals for α-NPD and TCTA, accumulated in two distance intervals: 1.2–1.6 nm [(a) and (c)] and 2.0–2.4 nm [(b) and (d)]. By construction, the stochastically modeled PDFs closely follow the simulated PDFs, including interesting molecule-specific features such as the double-peak structure for TCTA in the interval 2.0–2.4 nm, see Fig. 4(d), which is the cause of the large spread in transfer integrals observed in Fig. 3(b). We note that the procedure takes into account the important correlation between the distance and transfer integrals between sites, but no other correlations that might exist between the morphology and transfer integrals or between site energies and transfer integrals.

C. Mobility function

The hole mobility functions $\mu(T,c,F)$ for α-NPD and TCTA are obtained by solving the three-dimensional master equation in steady state for the hole occupational probabilities p_i of the sites in large boxes, in a similar way to that in Ref. [7]. The master equation takes into account the strong on-site Coulombic repulsion of charges by disallowing two

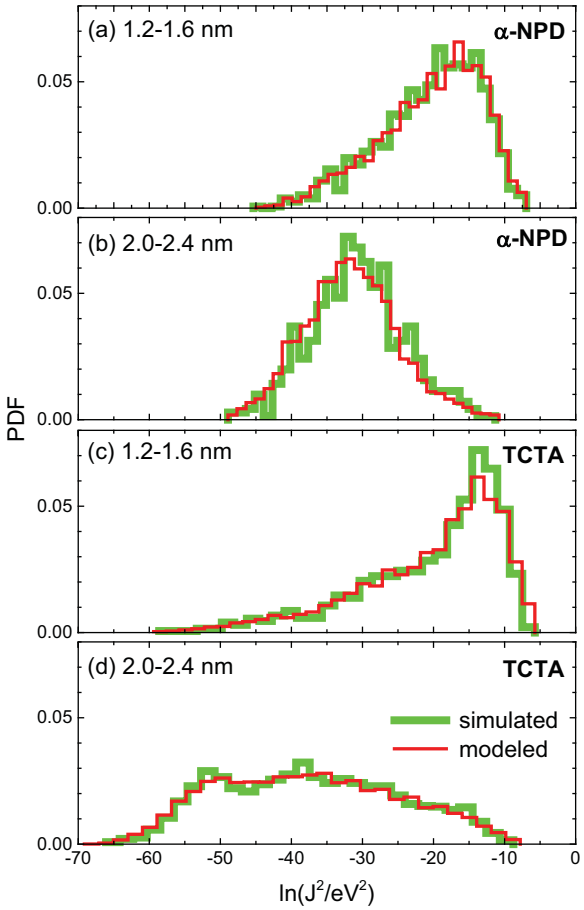

FIG. 4. *Ab initio* simulated and stochastically modeled PDF histograms of $\ln(J^2/\mathrm{eV}^2)$ for samples of α-NPD and TCTA within two different distance intervals, indicated by the shaded regions in Fig. 3. (a) and (c): 1.2–1.6 nm, (b) and (d): 2.0–2.4 nm. In both intervals about 10^3 simulated and about 10^6 modeled transfer integrals were considered.

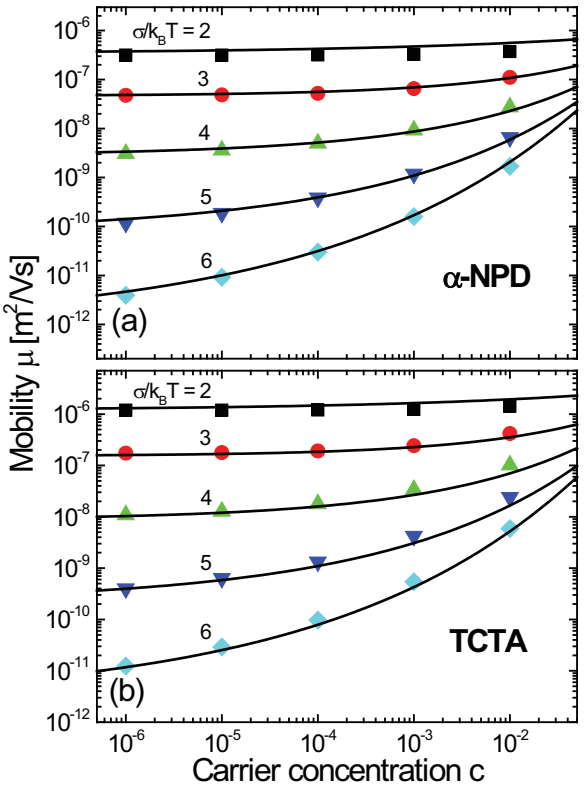

FIG. 5. Dependence of the zero-field ($F = 0$) hole mobility μ on the carrier concentration c for different temperatures T, in (a) α-NPD and (b) TCTA. Symbols: Results obtained by solving the master equation Eq. (3) for stochastically modeled morphologies and transfer integrals in cubic boxes, averaged over five disorder realizations. The error bar is of the order of the symbol size or smaller. Curves: Parametrization Eq. (4), with $\mu_0^* = 1.7 \times 10^{-6}$ m^2/V s, $C = 0.40$ (α-NPD) and $\mu_0^* = 6.1 \times 10^{-6}$ m^2/V s, $C = 0.41$ (TCTA).

charges to be on the same site. The site positions and transfer integrals are generated from the above stochastic models for the morphology and transfer integrals. The random site energies are drawn from a Gaussian distribution with standard deviation σ, where, on the basis of Fig. 1, we disregard any spatial correlation. The master equation (ME) in steady state is given by

$$\frac{dp_i}{dt} = \sum_{i \neq j} \left[\omega_{ji}\, p_j(1-p_i) - \omega_{ij}\, p_i(1-p_j)\right] = 0, \qquad (3)$$

where the rates ω_{ij} are given by Eq. (1). It is straightforward to obtain the charge-carrier mobility $\mu(T,c,F)$ from the solution of the ME.

The dependence of the resulting μ on temperature T and carrier concentration c is investigated in Fig. 5. The symbols in Figs. 5(a) and 5(b) are the ME results for μ at vanishing electric field $F = 0$ as a function of c at different values of $\hat{\sigma} \equiv \sigma/k_\mathrm{B}T$, for α-NPD and TCTA, respectively. We used simulation boxes up to $110 \times 110 \times 110$ nm^3 and performed averages over five disorder realizations. The curves represent the result of a fit to the data using the parametrization scheme given in Ref. [7]:

$$\mu(T,c) = \mu_0(T) \exp\left[\frac{1}{2}(\hat{\sigma}^2 - \hat{\sigma})(2c)^\delta\right],$$
$$\mu_0(T) = \mu_0^* \exp[-C\hat{\sigma}^2],$$
$$\delta \equiv 2\frac{\ln(\hat{\sigma}^2 - \hat{\sigma}) - \ln(\ln 4)}{\hat{\sigma}^2}, \qquad (4)$$

with $\mu_0^* = 1.7 \times 10^{-6}$ m^2/V s, $C = 0.40$ for α-NPD and $\mu_0^* = 6.1 \times 10^{-6}$ m^2/V s, $C = 0.41$ for TCTA. We note that the values for C are very close to the value $C = 0.42$ found for the EGDM [7], so that the T dependencies are very similar to the EGDM. The c dependence is the same as for the EGDM, in accordance with the conclusion in Ref. [11] that the c dependence at not too high c only depends on the shape of the DOS.

In Fig. 6 we investigate the dependence of μ on the electric field F for a low (main panels) and a high (insets) carrier concentration c at different values of $\hat{\sigma}$. The symbols are again the ME results. The curves represent the result of a fit to the data using the parametrization scheme given in

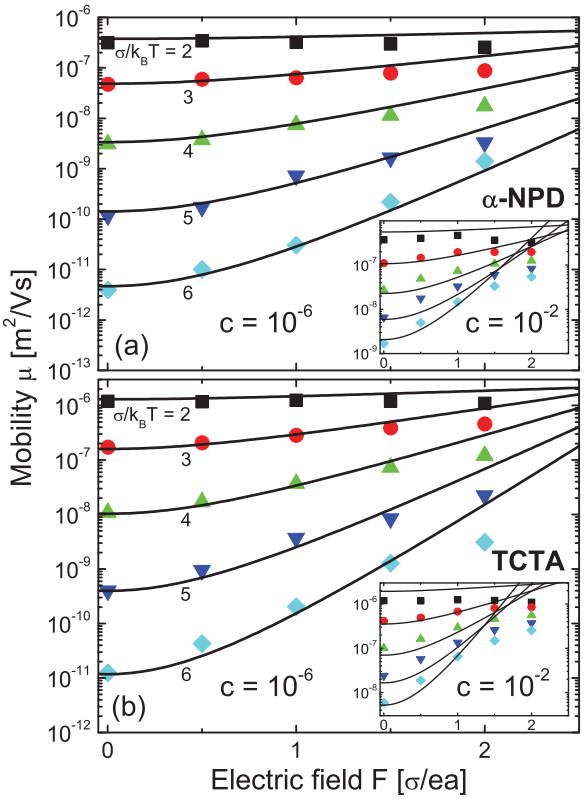

FIG. 6. Dependence of μ on the electric field F at a low (main panel) and high (inset) carrier concentration c for different temperatures T, in (a) α-NPD and (b) TCTA. Symbols: Master-equation results. Curves: Parametrization Eqs. (4) and (5), with $A = 0.30$, $B = 1.2$ (α-NPD) and $A = 0.32$, $B = 1.7$ (TCTA).

Ref. [7]:

$$\mu(T,c,F) = \mu(T,c) f(T,F),$$

$$f(T,F) = \exp\left[A(\hat{\sigma}^{3/2} - 2.2)\left(\sqrt{1 + B\left(\frac{Fea}{\sigma}\right)^2} - 1 \right) \right], \tag{5}$$

with $a \equiv N_t^{-1/3}$, and parameters $A = 0.30$, $B = 1.2$ for α-NPD and $A = 0.32$, $B = 1.7$ for TCTA. We note that, just like in the EGDM [7], the F and c dependencies are approximately uncoupled, as demonstrated by the approximately equal F dependence of μ at high and low c (compare the insets in Fig. 6 with the main panels). The compact parametrization deviates from the ME results for large F, but is sufficiently accurate in the experimentally relevant field range up to $eaF/\sigma \approx 1$. For the EGDM, the values $A = 0.44$ and $B = 0.8$ were used in the parametrization [7]. At small fields, when $\ln \mu$ is proportional to $AB F^2$, the factor AB characterizes the field sensitivity. This factor is equal to 0.36 and 0.54 for α-NPD and TCTA, respectively, while it is 0.35 for the EGDM. We therefore conclude that the F dependence of the mobility for α-NPD is very similar to the EGDM, whereas for TCTA it is somewhat stronger.

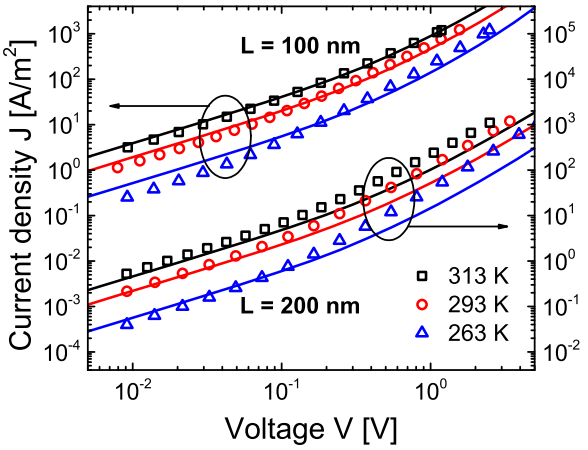

FIG. 7. Comparison of measured current density–voltage (J-V) characteristics of ITO|50 nm HTM:dopant|L α-NPD|50 nm HTM:dopant|Au|Al hole-only devices with $L = 100$ and 200 nm at different temperatures (symbols) and results obtained by solving a one-dimensional drift-diffusion (1D-DD) equation using the mobility function Eqs. (4) and (5) with $\sigma = 0.10$ eV (curves).

III. APPLICATION TO α-NPD HOLE-ONLY DEVICES

In this section we apply the *ab initio* mobility model of the previous section, given by its parametrization Eqs. (4) and (5), to two types of hole-only α-NPD devices. We compare measured current density–voltage (J-V) characteristics for different temperatures and α-NPD layer thicknesses to characteristics calculated with a standard one-dimensional drift-diffusion (1D-DD) model using the mobility model. This provides a very sensitive way to validate the model. We adopt the 1D-DD model and solution method of Ref. [34], which takes into account the dependence of the mobility μ on the local carrier concentration c and electric field F, and uses the generalized Einstein equation for the diffusion coefficient [35]. Such continuum 1D-DD modeling of single-carrier devices has been compared by us in the past with discrete 3D master-equation [36] and kinetic Monte Carlo modeling [37], and found to provide reliable J-V characteristics for even thinner organic layers than considered here.

The first type of device has the p-doped|intrinsic|p-doped (p-i-p) structure ITO|50 nm HTM:dopant|L α-NPD|50 nm HTM:dopant|Au|Al, where HTM:dopant is a combination of a hole-transporting material and a dopant (supplied by Novaled). In these devices the injection into the α-NPD layer is very efficient, which we take into account in the 1D-DD modeling by assuming the Gaussian DOS to be half filled at the interfaces between the α-NPD and the doped layers ($c = 0.5$).

The symbols in Fig. 7 give the measured J-V characteristics at different temperatures for such devices with α-NPD layer thicknesses of $L = 100$ and 200 nm. A proper 1D-DD modeling of the measured J-V characteristics using the parametrization of the α-NPD mobility of the previous section turned out not to be possible: the current densities are much too low and the T dependence of the J-V characteristics is much too strong. However, as demonstrated in Fig. 7 a fair description can be obtained by *only* reducing the calculated value of $\sigma = 0.13$ to $\sigma = 0.10$ eV. For comparison, at the

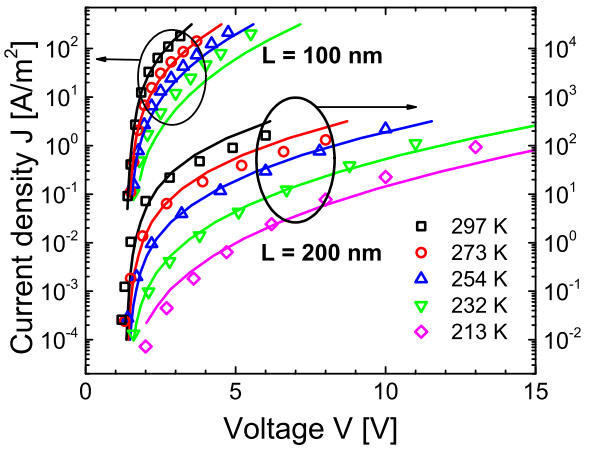

FIG. 8. Comparison of measured J-V characteristics of ITO|L α-NPD|Pd hole-only devices with $L = 100$ and 200 nm at different temperatures (symbols) and results obtained by solving a 1D-DD equation using the mobility function Eqs. (4) and (5) with $\sigma = 0.10$ eV (curves). The injection and collection barriers at the anode and cathode were taken to be $\phi_1 = 0.5$ eV and $\phi_2 = 2.0$ eV, respectively.

lowest considered temperature of 263 K a reduction of σ from 0.13 to 0.10 eV corresponds, using $C = 0.40$ in Eq. (4), to an increase of the zero-field mobility by a factor of about 200. The fact that *both* the magnitude of the current densities and the T dependence of the J-V characteristics is reproduced suggests that, apart from σ, the other aspects of the mobility function are well described.

We also studied the devices in Ref. [12], which have the structure ITO|L α-NPD|Pd. The energy barrier at the ITO anode makes these devices strongly injection-limited and therefore these devices behave quite differently from the above p-i-p devices. The J-V characteristics of these devices were modeled in Ref. [12], with both the EGDM and the ECDM. In that modeling, σ, N_t, an overall mobility prefactor μ_0^* [cf. Eq. (4)], and the barriers for hole injection at the ITO anode and the PD cathode, ϕ_1 and ϕ_2, respectively, were treated as parameters. With both the EGDM and the ECDM very good fits could be obtained, with $\sigma = 0.14 \pm 0.01$ eV, $N_t = (0.20 \pm 0.04) \times 10^{27}$ m^{-3} for the EGDM and $\sigma = 0.10 \pm 0.01$ eV, $N_t = (3.7 \pm 0.8) \times 10^{27}$ m^{-3} for the ECDM, and in both cases $\phi_1 = 0.4 \pm 0.1$ eV and $\phi_2 = 1.9 \pm 0.1$ eV. Since the experimental density $N_t = 1.4 \times 10^{27}$ m^{-3} is closer to the ECDM than to the EGDM value, it was suggested that the energetic disorder in α-NPD is spatially correlated. As Fig. 1 points at only a very a small amount of correlation in the energy disorder, we decided to remodel the J-V characteristics of these devices with the present mobility model.

The symbols in Fig. 8 give the measured J-V characteristics at different temperatures for these devices with α-NPD layer thicknesses of $L = 100$ and 200 nm. In the 1D-DD modeling we took into account the image charges in the metallic electrodes and the barriers for hole injection at the ITO anode and the Pd cathode in the same way as in Ref. [12]. Like for the p-i-p devices, a proper modeling with $\sigma = 0.13$ eV was not possible, but again a fair description can be obtained by *only* reducing σ to 0.10 eV. At the lowest considered temperature of 213 K this now corresponds to an increase of the zero-field mobility by a factor of about 3600. The values used for ϕ_1 and ϕ_2 to obtain an optimal fit differ slightly from Ref. [12]: $\phi_1 = 0.5$ and $\phi_1 = 2.0$ eV. We note that we were not able to obtain converged 1D-DD results with our method for a temperature lower than 232 K for the device with $L = 100$ nm and lower than 213 K for the device with $L = 200$ nm, so that we cannot compare our modeled results with the results at the very lowest temperatures reported in Ref. [12].

Although the agreement between measured and modeled results in Fig. 8 is not as good as in the modeling of Ref. [12] (which was carried out using N_t and μ_0^* as extra fit parameters in comparison to the present modeling), the agreement is certainly satisfactory. We note that the satisfactory agreement is partly caused by the higher injection barrier of $\phi_1 = 0.5$ eV at the ITO contact, instead of the $\phi_1 = 0.4$ eV used in Ref. [12]. The value $\phi_1 = 0.5$ is more compatible with the expected range of 0.4–0.9 eV, based on the nominal vacuum work function of 4.7–5.0 eV of ITO and the HOMO energy of 5.4–5.6 eV of α-NPD [12]. We conclude that a satisfactory agreement between measured and modeled J-V characteristics can be obtained with the present mobility model, without assuming correlation in the energy disorder.

IV. DISCUSSION AND CONCLUSIONS

In this work an *ab initio* mobility model has been developed for α-NPD and TCTA. For α-NPD, a consistent picture of the hole mobility function has been obtained, which is expected to also hold for other amorphous molecular semiconductors. The only adjustment made was a slight decrease of the calculated value of the energetic disorder strength σ.

We conclude that a proper modeling of the J-V characteristics of different types of α-NPD devices is possible with uncorrelated energy disorder, contrary to the suggestion in Ref. [12] that the energy disorder in α-NPD is correlated. Further studies of charge transport in other amorphous molecular semiconductors should show how general this conclusion is. It clearly does not hold for molecular semiconductors with large molecular dipole moments, such as Alq_3. Also, energy disorder in the hole transporter DPBIC (tris[(3-phenyl-1H-benzimidazol-1-yl-2(3H)-ylidene)-1,2-phenylene]Ir), which also has a dipole moment, is correlated, but not as strongly as in the ECDM [20]. It can be seen in Fig. 1 that, despite their vanishing dipole moment, in α-NPD and TCTA a small amount of correlation is still present. In future work we will address the question of whether taking into account this small amount of correlation can further improve the agreement with experiment. In particular, we will investigate whether the somewhat stronger voltage dependence of the current density observed at low temperatures in both considered types of devices (see Figs. 7 and 8) can be explained by a field dependence that is slightly enhanced by this correlation.

The present study provides a clear answer to the question of why the GEMM in Ref. [19] seems to correctly explain the T dependence of the mobility, while it predicts $C = 0.25$ in the T dependence of the mobility in Eq. (4) instead of the values $C = 0.40$ (α-NPD) and 0.41 (TCTA) found in the present study. The too large values of σ in Ref. [19] are compensated by the too small value of C, leading to a proper T dependence

of the mobility. This is another indication that the value of σ obtained from the *ab initio* simulations is too large.

A standard technique to obtain charge-carrier mobilities is the use of time-of-flight (TOF) measurements. We note, however, that one should be very careful in comparing absolute values of calculated mobilities with mobilities obtained from TOF measurements. Because of the dispersive transport, the arrival time of carriers at the collecting electrode in TOF experiments has a significant spread. Also, TOF devices are in general quite thick ($\sim$10 μm), so that one may ask to what extent the structure is the same as for the presently studied very thin (100–200 nm) devices. Furthermore, the excitation of carriers in the DOS at the illuminated electrode and the carrier-concentration (c) dependence of the mobility can lead to an overestimation of the mobility. In fact, taking the value $\sigma = 0.10$ eV obtained from the modeling of the α-NPD devices in the previous section and the values $\mu_0^* = 1.7 \times 10^{-6}$ m^2/V s and $C = 0.40$, we obtain from Eq. (4) a mobility of 2.9×10^{-9} m^2/V s in the limit of vanishing carrier concentration and electric field, which is an order of magnitude smaller than the reported TOF value of 3×10^{-8} m^2/V s [38]. The device studies in the present paper provide in our opinion a more reliable and comprehensive validation of the mobility function.

It is encouraging to see that, despite the large difference in their molecular structure, the parametrization scheme of the mobility function given by Eqs. (4) and (5) is valid for both considered amorphous semiconductors, α-NPD and TCTA. This suggests that the mobility function has a general validity and could be broadly applicable to organic device modeling. We conclude that the T and c dependencies of the mobility in the original EGDM were very well described, despite the drastic simplifications underlying this lattice-based model. The EGDM description of the F dependence is found to be qualitatively correct for both investigated semiconductors. In the case of α-NPD, the EGDM happens to even provide a quantitatively accurate F dependence.

The question remains why the *ab initio* simulations overestimate the value of σ. In order to answer this question, we plan to critically examine the key ingredients of the *ab initio* approach, such as the force fields used to generate the morphology and the transferability of the molecular structures generated at the molecular mechanics level to the subsequent quantum treatment.

ACKNOWLEDGMENTS

We thank Dr. Velimir Meded and Prof. Dr. René Janssen for stimulating discussions. The research is part of the Dutch-German project "Modeling of organic light-emitting diodes: From molecule to device" (MODEOLED). On the Dutch side, it is supported by the Dutch Technology Foundation STW, the applied science division of NWO, and the Technology Program of the Dutch Ministry of Economic Affairs (Project No. 12200). On the German side it is supported by the "Deutsche Forschungsgemeinschaft" (DFG; Project No. WE1863/22-1). The *ab initio* microscopic simulations were performed on the computational resource ForHLR Phase I, funded by the German Ministry of Science, Research, and the Arts Baden-Württemberg, and the DFG. The work was carried out in part at the Philips Research Laboratories, Eindhoven, The Netherlands (R.C.).

[1] H. Bässler, Phys. Status Solidi (b) **175**, 15 (1993).
[2] Y. Gartstein and E. Conwell, Chem. Phys. Lett. **245**, 351 (1995).
[3] S. V. Novikov, D. H. Dunlap, V. M. Kenkre, P. E. Parris, and A. V. Vannikov, Phys. Rev. Lett. **81**, 4472 (1998).
[4] S. Baranovskii, I. Zvyagin, H. Cordes, S. Yamasaki, and P. Thomas, Phys. Status Solidi (b) **230**, 281 (2002).
[5] Y. Roichman and N. Tessler, Synth. Met. **135**, 443 (2003).
[6] C. Tanase, E. J. Meijer, P. W. M. Blom, and D. M. de Leeuw, Phys. Rev. Lett. **91**, 216601 (2003).
[7] W. F. Pasveer, J. Cottaar, C. Tanase, R. Coehoorn, P. A. Bobbert, P. W. M. Blom, D. M. de Leeuw, and M. A. J. Michels, Phys. Rev. Lett. **94**, 206601 (2005).
[8] R. Coehoorn, W. F. Pasveer, P. A. Bobbert, and M. A. J. Michels, Phys. Rev. B **72**, 155206 (2005).
[9] M. Bouhassoune, S. L. M. van Mensfoort, P. A. Bobbert, and R. Coehoorn, Org. Electron. **10**, 437 (2009).
[10] J. Cottaar, L. J. A. Koster, R. Coehoorn, and P. A. Bobbert, Phys. Rev. Lett. **107**, 136601 (2011).
[11] J. Cottaar, R. Coehoorn, and P. A. Bobbert, Phys. Rev. B **85**, 245205 (2012).
[12] S. L. M. van Mensfoort, V. Shabro, R. J. de Vries, R. A. J. Janssen, and R. Coehoorn, J. Appl. Phys. **107**, 113710 (2010).
[13] A. Miller and E. Abrahams, Phys. Rev. **120**, 745 (1960).
[14] L. Pautmeier, R. Richert, and H. Bässler, Synth. Met. **37**, 271 (1990).
[15] J. J. Kwiatkowski, J. Nelson, H. Li, J. L. Bredas, W. Wenzel, and C. Lennartz, Phys. Chem. Chem. Phys. **10**, 1852 (2008).
[16] V. Rühle, A. Lukyanov, F. May, M. Schrader, T. Vehoff, J. Kirkpatrick, B. Baumeier, and D. Andrienko, J. Chem. Theory Comput. **7**, 3335 (2011).
[17] A. Fuchs, T. Steinbrecher, M. S. Mommer, Y. Nagata, M. Elstner, and C. Lennartz, Phys. Chem. Chem. Phys. **14**, 4259 (2012).
[18] T. Neumann, D. Danilov, C. Lennartz, and W. Wenzel, J. Comput. Chem. **34**, 2716 (2013).
[19] P. Friederich, F. Symalla, V. Meded, T. Neumann, and W. Wenzel, J. Chem. Theory Comput. **10**, 3720 (2014).
[20] P. Kordt, J. J. M. van der Holst, M. Al Helwi, W. Kowalsky, F. May, A. Badinski, C. Lennartz, and D. Andrienko, Adv. Funct. Mater. **25**, 1955 (2015).
[21] V. Rodin, F. Symalla, V. Meded, P. Friederich, D. Danilov, A. Poschlad, G. Nelles, F. von Wrochem, and W. Wenzel, Phys. Rev. B **91**, 155203 (2015).
[22] A. Massé, R. Coehoorn, and P. A. Bobbert, Phys. Rev. Lett. **113**, 116604 (2014).
[23] B. Baumeier, O. Stenzel, C. Poelking, D. Andrienko, and V. Schmidt, Phys. Rev. B **86**, 184202 (2012).
[24] P. Kordt, O. Stenzel, B. Baumeier, V. Schmidt, and D. Andrienko, J. Chem. Theory Comput. **10**, 2508 (2014).
[25] M. Mesta, M. Carvelli, R. J. de Vries, H. van Eersel, J. J. M. van der Holst, M. Schober, M. Furno, B. Lüssem, K. Leo, P.

Loebl, R. Coehoorn, and P. A. Bobbert, Nat. Mater. **12**, 652 (2013).
[26] R. A. Marcus, Rev. Mod. Phys. **65**, 599 (1993).
[27] P.-O. Löwdin, J. Chem. Phys. **18**, 365 (1950).
[28] V. Stehr, J. Pfister, R. F. Fink, B. Engels, and C. Deibel, Phys. Rev. B **83**, 155208 (2011).
[29] R. Ahlrichs, M. Bär, M. Häser, H. Horn, and C. Kölmel, Chem. Phys. Lett. **162**, 165 (1989).
[30] A. D. Becke, J. Chem. Phys. **98**, 1372 (1993).
[31] A. Schäfer, H. Horn, and R. Ahlrichs, J. Chem. Phys. **97**, 2571 (1992).
[32] S. F. Nelsen, S. C. Blackstock, and Y. Kim, J. Am. Chem. Soc. **109**, 677 (1987).
[33] A. Schäfer, C. Huber, and R. Ahlrichs, J. Chem. Phys. **100**, 5829 (1994).
[34] S. L. M. van Mensfoort and R. Coehoorn, Phys. Rev. B **78**, 085207 (2008).
[35] Y. Roichman and N. Tessler, Appl. Phys. Lett. **80**, 1948 (2002).
[36] J. J. M. van der Holst, M. A. Uijttewaal, B. Ramachandhran, R. Coehoorn, P. A. Bobbert, G. A. de Wijs, and R. A. de Groot, Phys. Rev. B **79**, 085203 (2009).
[37] J. J. M. van der Holst, F. W. A. van Oost, R. Coehoorn, and P. A. Bobbert, Phys. Rev. B **83**, 085206 (2011).
[38] C. H. Cheung, K. K. Tsung, K. C. Kwok, and S. K. So, Appl. Phys. Lett. **93**, 083307 (2008).